not be detected. We therefore infer that when the substrate is heated, the nanotube and onion structures disintegrate on impact far more efficiently and to a greater extent.

Tetrahedral amorphous carbon has been the hardest form of non-diamond carbon thin film obtained to date. The hardness and elastic recovery measured from indentation curves (with a 5 mN maximum loading) on similar-thickness films—500 nm—of nanoparticle carbon (NC) and tetrahedral amorphous carbon are shown in Table 1. A typical indentation characteristic of an NC film deposited at 350 °C is shown in Fig. 3. The absence of large nanotube regions in this film, compared to the films deposited at room temperature, and the fact that it has a high hardness and elastic recovery, suggest that a qualitatively new form of carbon thin film is obtained.

Considering the difference between the NC films deposited at room temperature and high temperature in terms of mechanical properties, it is possible that breakup of the large nanotube regions results in a denser structure without the weak interplanar coupling of the curved hexagonal planes. It seems reasonable to suppose that by heating the substrate the C atoms become more mobile, and thus interlinking becomes more prevalent as the tubes break up into smaller fragments. In the resulting film, fine structure would not be easily distinguishable from the surrounding amorphous matrix (spectrum d in Fig. 2). Although insight into the detailed structure of superhard and superelastic nanoparticle carbon nanoparticle carbon films requires further experimental and theoretical study, their relative ease of deposition makes them particularly suitable for evaluation as protective coatings in applications ranging from computer memory disks to surgical implants. □

Received 15 April; accepted 21 August 1996.

1. Sjostrom, H., Stafstrom, S., Roman, M. & Sundgren, J.-F. *Phys. Rev. Lett.* **75,** 1336–1339 (1995).
2. McKenzie, D. R., Muller, D. & Pailthrope, B. A. *Phys. Rev. Lett.* **67,** 773–776 (1991).
3. Fallon, P. J. *et al. Phys. Rev. B* **48,** 4777-4782 (1993).
4. Charrier, C. *et al. Diamond Relat. Mater.* **3,** 41–46 (1994).
5. Iijima, S. *Nature* **354,** 56–57 (1991).
6. Ugarte, D. *Nature* **359,** 707–709 (1992).
7. Rogozin, A. & Fontana, R. Paper presented at *Int. Congr. Thin Films & Metallurgical Coatings*, San Diego, April, 1996.
8. Gamalay, E. G. & Ebbesen, T. W. *Phys. Rev. B* **52,** 2083–2089 (1995).
9. Berger, S. D., McKenzie, D. R. & Martin, P. J. *Phil. Mag. Lett.* **57,** 285–288 (1988).
10. Despres, J. F., Daguerre, E. & Lafdi, K. *Carbon* **33,** 87–92 (1995).
11. Iijima, S., Brabec, C., Maiti, A. & Bernholc, J. *J. Chem. Phys.* **104,** 2089–2092 (1996).

ACKNOWLEDGEMENTS. We thank R. Keyse for EELS measurements, J. Yuan and S. R. P. Silva for discussion, and R. Fontana and P. Hatto for support of this work.

CORRESPONDENCE should be addressed to G.A.J.A. (e-mail: ga@liv.ac.uk).

Scaling behaviour of heartbeat intervals obtained by wavelet-based time-series analysis

Plamen Ch. Ivanov*, Michael G. Rosenblum*, C.-K. Peng*†, Joseph Mietus†, Shlomo Havlin*‡, H. Eugene Stanley* & Ary L. Goldberger†

* Center for Polymer Studies and Department of Physics, Boston University, Boston, Massachusetts 02215, USA
† Cardiovascular Division, Harvard Medical School, Beth Israel Hospital, Boston, Massachusetts 02215, USA
‡ Gonda-Goldschmied Center and Department of Physics, Bar-Ilan University, Ramat Gan, 52900 Israel

Biological time-series analysis is used to identify hidden dynamical patterns which could yield important insights into underlying physiological mechanisms. Such analysis is complicated by the fact that biological signals are typically both highly irregular and non-stationary, that is, their statistical character changes slowly or intermittently as a result of variations in background influences[1–3]. Previous statistical analyses of heartbeat dynamics[4–6] have identified long-range correlations and power-law scaling in the normal heartbeat, but not the phase interactions between the different frequency components of the signal. Here we introduce a new approach, based on the wavelet transform and an analytic signal approach, which can characterize non-stationary behaviour and elucidate such phase interactions. We find that, when suitably rescaled, the distributions of the variations in the beat-to-beat intervals for all healthy subjects are described by a single function stable over a wide range of timescales. However, a similar scaling function does not exist for a group with cardiopulmonary instability caused by sleep apnoea. We attribute the functional form of the scaling observed in the healthy subjects to underlying nonlinear dynamics, which seem to be essential to normal heart function. The approach introduced here should be useful in the analysis of other nonstationary biological signals.

A random process is stationary if its statistical characteristics are invariant under time shifts, that is, if they remain the same when t is replaced by $t + \Delta$, where Δ is arbitrary. The probability densities, together with the moment and correlation functions, do not then depend on the absolute position of the points on the time axis, but only on their relative configuration. Non-stationarity, an important aspect of biological variability, can be associated with patterns of different drifts in the mean value of a given signal, or with changes in its variance which may be gradual or abrupt. Time series of beat-to-beat (R–R) heart-rate intervals (Fig. 1*a*), obtained from digitized electrocardiograms, are known to be non-stationary and exhibit extremely complex behaviour[7]. A typical feature of such non-stationary signals is the presence of 'patchy' patterns that change over time (Fig. 1*b*). Heterogeneous properties may be even more strongly expressed in certain cases of abnormal heart activity. Traditional approaches (such as the power spectrum and correlation analysis[4,8,9]) are not suited for such non-stationary (patchy) sequences, nor do they carry information stored in the Fourier phases which is crucial for determining nonlinear characteristics.

To address these problems, we present an alternative method, which we call 'cumulative variation amplitude analysis', to study the subtle structure of physiological time series. This method involves the sequential application of a set of algorithms based on wavelet and Hilbert transform analysis. First, we apply the wavelet transform (Fig. 1*c*), because it does not require stationarity and preserves the Fourier phase information. The wavelet transform[10–12] of a time series $s(t)$ is defined as

$$T_{\psi}(t_0, a) \equiv \frac{1}{a}\int_{-\infty}^{+\infty} s(t)\psi\left(\frac{t - t_0}{a}\right)\mathrm{d}t \qquad (1)$$

where the analysing wavelet ψ has a width of the order of the scale a, and is centred at time t_0. The wavelet transform T is sometimes called a 'mathematical microscope' because it allows the study of properties of the signal on any chosen scale a. For high frequencies (small a), the ψ functions have good localization (being effectively non-zero only on small sub-intervals), so short-time regimes or high-frequency components can be detected by the wavelet analysis. However, a wavelet with too large a value of scale

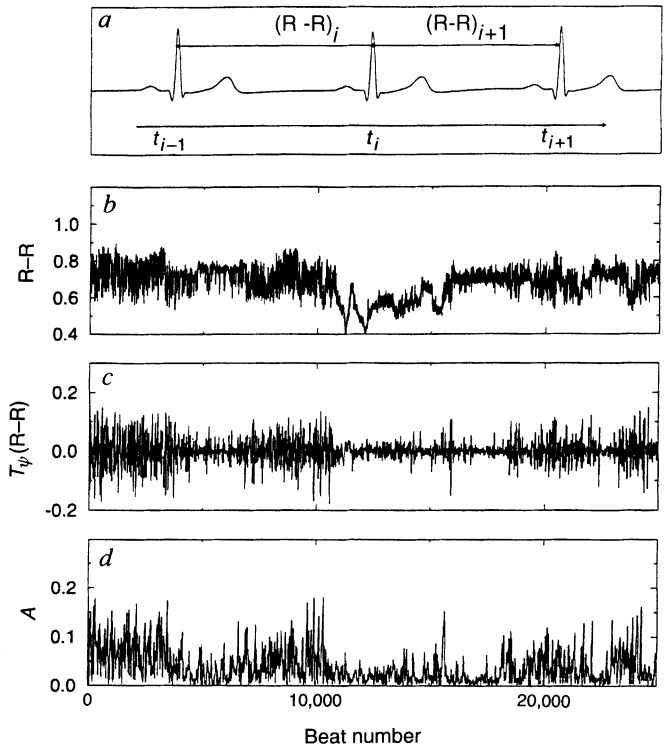

FIG. 1 *a*, Segment of electrocardiogram showing beat-to-beat $(R–R)_i$ intervals. *b*, Plot of R–R time series against consecutive beat number for a period of 6 h ($\sim 2.5 \times 10^4$ beats). Non-stationarity (patchiness) is evident over both long and short timescales. Although these patches clearly differ in the amplitude and frequency of variations, their quantitative characterization remains an open problem. *c*, Wavelet transform T_ψ(R–R) of the R–R signal in *b*. Non-stationarities related to constants and linear trends have been filtered. The first derivative of the gaussian $\psi^{(1)}$ is orthogonal to segments of the time series with different constant local average. This results in fluctuations of the wavelet transform values around zero, with highest spikes at the positions where a sharp transition in the constant value in the constant value occurs. Thus the large spikes indicate the boundaries between patterns with different local average in the signal, and the smaller fluctuations represent variations of the signal within a given dynamical regime. Because $\psi^{(1)}$ is not orthogonal to linear (non-constant) trends, the presence of consecutive linear trends in the R–R intervals will give rise to fluctuations of the wavelet transform values around different non-zero levels corresponding to the slopes of the linear trends. $\psi^{(2)}$ and higher order derivatives can eliminate the influence of linear as well as nonlinear trends in the fluctuations of the wavelet transform values. *d*, Instantaneous amplitudes $A(t)$ of the wavelet transform signal in *c*; $A(t)$, calculated using the Hilbert transform, measures the cumulative variations in the interbeat intervals over an interval proportional to the wavelet scale *a*.

a (low frequency) will filter out almost the entire frequency content of the time series, thus losing information about the intrinsic dynamics of the system. We focus our 'microscope' on scale $a = 8$ beats, which smoothes locally very high-frequency variations, and best probes patterns of specific duration (30 s to 1 min) (see Fig. 2 legend). The wavelet transform can eliminate local polynomial behaviour (trends) in the non-stationary signal by an appropriate choice of the analysing wavelet ψ (ref. 13). In our study we use derivatives of the gaussian function: $\psi^{(n)} \equiv \mathrm{d}^n/\mathrm{d}t^n \mathrm{e}^{-\frac{1}{2}t^2}$.

The wavelet transform is thus a cumulative measure of the variations in the heart-rate signal over a region proportional to the wavelet scale, so study of the behaviour of the wavelet values can reveal intrinsic properties of the dynamics that are masked by non-stationarity.

The next step of the cumulative variation amplitude analysis is to extract the amplitudes of the variations in the beat-to-beat signal, by means of an analytic signal approach[8,14] that also does not require stationarity. Let $s(t)$ represent an arbitrary signal. The analytic signal, a complex function of time, is defined by $S(t) \equiv s(t) + i\tilde{s}(t) = A(t)\mathrm{e}^{i\phi(t)}$, where $\tilde{s}(t)$ is the Hilbert transform[15] of $s(t)$, $A(t) \equiv \sqrt{s^2(t) + \tilde{s}^2(t)}$ is the amplitude, and $\phi(t) \equiv \tan^{-1}(\tilde{s}(t)/s(t))$ is the phase.

We studied the distribution of the amplitudes of the beat-to-beat variations (Fig. 1*d*) for a group of healthy subjects ($N = 18, 5$ males and 13 females; age, 20–50 years, mean 34 years) and a group of subjects[16] with obstructive sleep apnoea[17] ($N = 16$ males; age, 32–56 years, mean 43 years). To minimize non-stationarity resulting from changes in the level of activity, we begin by considering night-phase (0:00 to 6:00) records of interbeat intervals ($\sim 10^4$ beats) for both groups. Inspection of the distribution functions of the amplitudes of the cumulative variations indicates marked differences between individuals (Fig. 2*a*). These differences are not surprising, given the underlying physiological differences among healthy subjects.

We next analyse the distributions of the beat-to-beat variation amplitudes. For the healthy group, these are well fit by the generalized homogeneous form[18] (the gamma distribution)

$$P(x,b) = \frac{b^{v+1}}{\Gamma(v+1)} x^v \mathrm{e}^{-bx} \tag{2}$$

where $b \equiv v/x_0$, $\Gamma(v+1)$ is the gamma function, x_0 is the position of the peak $P = P_{\max}$, and v is the fitting parameter (Fig. 3*a*). A function $P(x,b)$ is a generalized homogeneous function if there exist two numbers α and β, called scaling powers, such that, for all positive values of the parameter λ,

$$P(\lambda^\alpha x, \lambda^\beta b) = \lambda P(x,b) \tag{3}$$

Generalized homogeneous functions are defined as solutions of this functional equation; $P(x,b)$ satisfies this equation with $\alpha = -1$ and $\beta = 1$.

Functions describing physical systems near their critical points are generalized homogeneous functions[19]. Data collapse is one of the important properties of generalized homogeneous functions: instead of data points falling on a family of curves, one for each value of b, data points collapse onto a single curve given by the scaling function

$$\tilde{P}(u) \equiv P(x,b)/b \tag{4}$$

where the number of independent variables is reduced by defining the scaled variable $u \equiv bx$. Our results show that a common scaling function $\tilde{P}(u)$ defines the probability density of the magnitudes of the variations in the beat-to-beat intervals for each healthy subject. Note that it is sufficient to specify only one parameter b to characterize the heterogeneous heartbeat variations for each subject in this group.

To test the hypothesis that there is a hidden, possibly universal, structure to these heterogeneous time series, we rescale the distributions and find for all healthy subjects that the data conform to a single scaled plot ('data collapse') (Fig. 2*b*). Such behaviour is reminiscent of a wide class of well-studied physical systems with universal scaling properties[19,20]. In contrast, the subjects with sleep apnoea show individual probability distributions (Fig. 2*c*) which fail to collapse (Fig. 2*d*).

We also analysed heart-rate dynamics for the healthy subjects during daytime hours (12:00 to 18:00). Our results indicate that the observed, apparently universal behaviour holds not only for the night phase but also for the day phase (Fig. 3*b*). Moreover, we find the observed scaling to be stable for a wide range of timescales (Fig. 3*c*).

To ascertain whether the observed scaling of the distributions for healthy subjects is an intrinsic property of normal heartbeat dynamics, we test the cumulative variation amplitude method on artificially generated signals with known properties. Our analysis of uniformly distributed random numbers in the interval [0,1] and of gaussian-distributed noise with and without long-range power-law correlations shows that, after the wavelet transform, the amplitude distributions follow the Rayleigh probability distribution $(x/\sigma^2)\mathrm{e}^{-x^2/\sigma^2}$. This finding agrees with the central limit theorem,

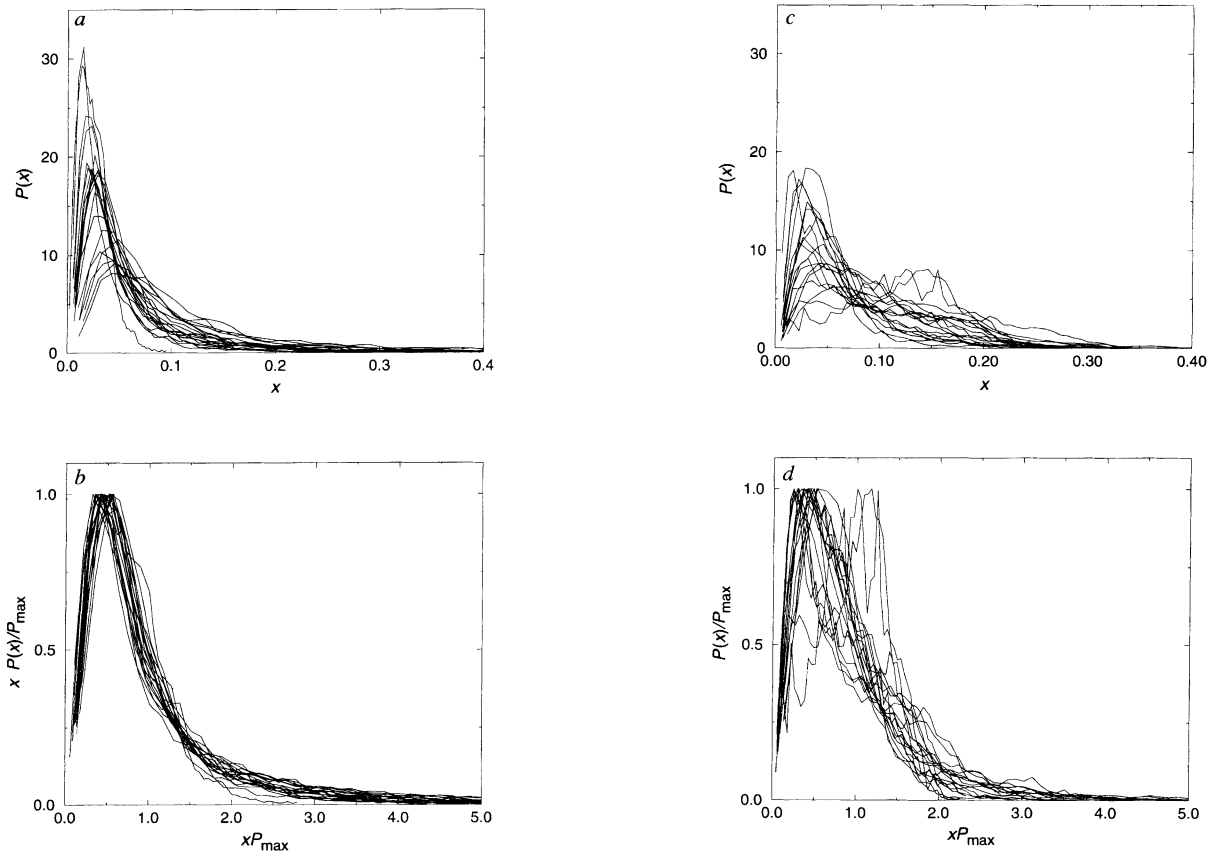

FIG. 2 *a*, Probability distributions $P(x)$ of the amplitudes of heart-rate variations $x \equiv A(t)$ for a group of 18 healthy adults. Individual differences are indicated by the different average value and widths (standard deviations) of these distributions. All distributions are normalized to unit area. *b*, Same probability distributions as *a*, after rescaling $P(x)$ by P_{max}, and x by $1/P_{max}$, to preserve the normalization to unit area. This rescaling is equivalent to that discussed in the text (equation (4)), as $P(x) \equiv P(x, b)$ and $P_{max} \propto b$. The data points collapse onto a single curve. *c*, Probability distributions for a group of 16 subjects with obstructive sleep apnoea. The second (right-hand) peak in the distributions for the sleep-apnoea subjects corresponds to the transient emergence of characteristic pathological oscillations in the heart rate associated with periodic breathing[6,17]. *d*, Distributions for the apnoea group after the same rescaling as in *b*. The absence of data collapse demonstrates deviation from normal heart behaviour. Direct analysis of interbeat interval histograms does not lead to data collapse or separation between the healthy and apnoea group. Moreover, the direct application of the Hilbert transform yielding the probability distribution of the instantaneous amplitudes of the original signal does not distinguish clearly healthy from abnormal cardiac dynamics. Hence the crucial feature of the wavelet transform is that it extracts dynamical properties hidden in the cumulative variations. For the healthy group, good data collapse is observed with a stable scaling form for wavelet scales $a = 2$ up to $a = 2$ up to $a = 64$. However, for very small scales ($a = 1, 2$), the average of the rescaled distributions of the apnoea group is indistinguishable from the average of the rescaled distributions of the healthy group. Hence very high frequencies are equally present in the signals from both groups. Our analysis yields the most robust results when *a* is tuned to probe the collective properties of patterns with a duration of 30 s to 1 min in the time series ($a = 8, 10$). The subtle difference in the tail of the distributions between day and night phases is also best seen for this scale range (Fig. 3).

which can be expressed as a property of convolutions (in our case wavelet transform): the convolution of a large number of positive functions is approximately a gaussian function, and the instantaneous amplitudes of a gaussian process follow the Rayleigh probability distribution[21].

We perform parallel analysis on surrogate data obtained from a healthy subject by Fourier transforming the original time series, preserving the amplitudes of the Fourier transform but randomizing the phases, and performing an inverse Fourier transform (Fig. 4). Thus both the original and surrogate signals have identical power spectra. Application of the cumulative variation amplitude analysis on this surrogate signal results again in a Rayleigh distribution, whereas the original time series has a distribution with an exponential tail. This test clearly indicates the important role of phase correlations in the R–R time series. The presence of these correlations is probably related to the underlying nonlinear dynamics. A characteristic feature of nonlinear (as opposed to linear) systems is the coupling of their components. These mode interactions may lead to non-random phase structure, and, in the context of the heartbeat, may account for the visually 'patchy' appearance of the normal time series. Our procedure, by preserving the collective phase properties of the original signal which cannot be detected by conventional power-spectrum analysis, uncovers a previously unknown nonlinear feature of healthy heart-rate fluctuations.

Furthermore, our finding suggests that, for healthy individuals, there may be a common structure to this nonlinear phase interaction. This scaling property cannot be explained by activity, as we analysed data from subjects during nocturnal hours, or by sleep stage transitions, as we found a similar pattern during daytime hours. The basis of this robust temporal structure remains unknown and presents a new challenge to understanding nonlinear mechanisms of heartbeat control. We also find that subjects with sleep apnoea, a common and important instability of cardiopulmonary regulation, show a dramatic alteration in the scaling pattern that may be related to pathologic mode locking associated with periodic breathing dynamics[22].

We believe that the method developed here can pick up differences that are missed by other approaches for two reasons: it can 'filter out' dominant features related to non-stationarities and thereby become sensitive to hidden scaling features; and is sensitive to the time ordering of events (provided a sensible choice

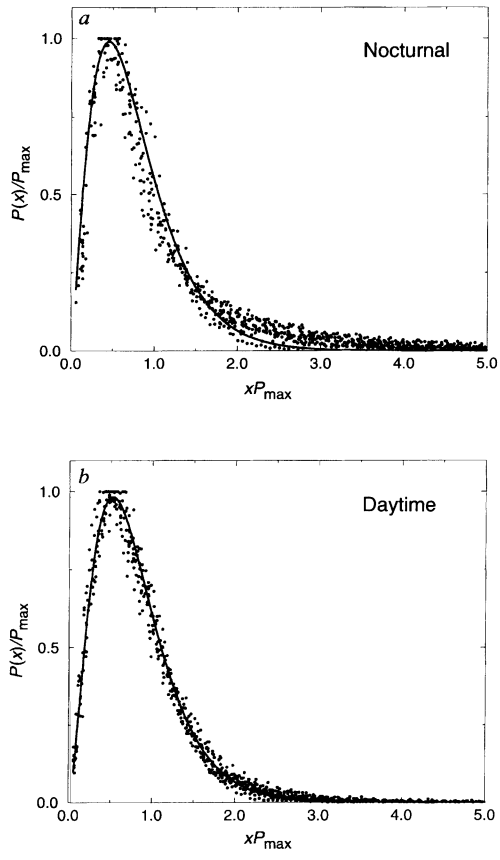

FIG. 3 *a*, The solid line is a fit of the rescaled distributions of the beat-to-beat variation amplitudes of the 18 healthy subjects during sleep hours to a stable gamma distribution with $\nu = 1.4 \pm 0.1$ (note that the stable gamma form has been used previously in the literature to describe other processes, such as the spike activity of a single neuron in ref. 23). *b*, Data for 6-h records of R–R intervals for the day phase of the same control group of 18 healthy subjects demonstrate similar scaling behaviour with a gamma distribution and $\nu = 1.8 \pm 0.1$, showing that the observed common structure for the healthy heart dynamics is not confined to the nocturnal phase. Semilog plots of the averaged distributions show a systematic deviation from the exponential form (slower decay) in the tails of the night-phase distributions, whereas the day-phase distributions follow the exponential form over almost the entire range. The tail of the observed distribution for the night phase indicates higher probability of larger variations in the healthy heart dynamics during sleep hours in comparison with the daytime dynamics. The maximum difference between the cumulative distributions of the individual subjects and the gamma fit in *a*, evaluated using the Kolmogorov–Smirnov test, can be a good index to separate the healthy from the apnoea group. Analysis of the mean and the variance of the individual distributions also shows clear separation for both groups. *c*, Average of the rescaled distributions for the amplitudes of the cumulative variations for the healthy group during nocturnal hours. Note that the observed gamma scaling is stable for a wide range of the wavelet transform scales *a*.

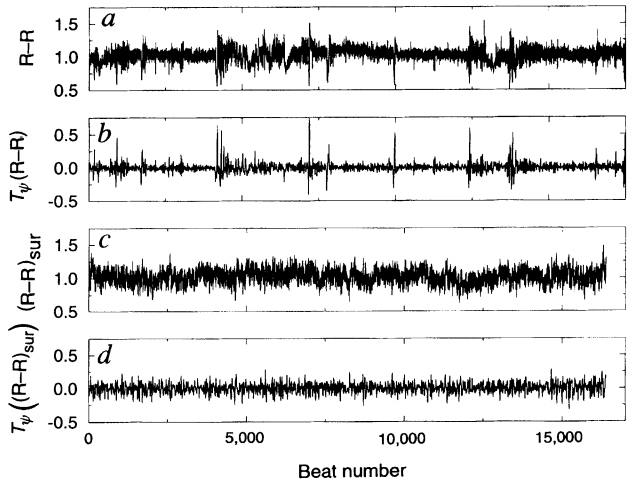

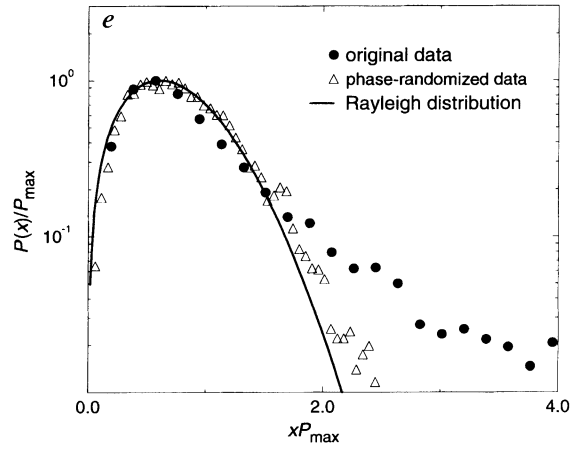

FIG. 4 *a*, Original R–R time series as a function of beat number. *b*, Wavelet transform T_ψ (R–R) of this series. *c*, Surrogate $(R–R)_{sur}$ signal after phase randomization. *d*, Wavelet transform of the surrogate signal which is more homogeneous (less patchy) than in *b*. *e*, Probability distributions of the amplitudes of variations after wavelet transform of the original and surrogate signals, as well as the theoretical Rayleigh distribution. The theoretical Rayleigh agrees with the distribution of the wavelet transform of the surrogate signal with randomized phases.

is made for the scale parameter *a*). Thus the dual use of wavelet and Hilbert transform techniques may be of practical diagnostic and prognostic value, and can be applied to a wide range of heterogeneous, 'real world' physiological signals. □

Received 7 February; accepted 22 August 1996.

1. Box, G. E. P., Jenkins, G. M. & Reinsel, G. C. *Time Series Analysis: Forecasting and Control* (Prentice-Hall, Englewood Cliffs, NJ, 1994).
2. Shlesinger, M. F. *Ann. NY Acad. Sci.* **504,** 214–228 (1987).
3. Liebovitch, L. S. *Biophys. J.* **55,** 373–377 (1989).
4. Bassingthwaighte, J. B., Liebovitch, L. S. & West, B. J. *Fractal Physiology* (Oxford Univ. Press, New York, 1994).
5. Peng, C.-K., Havlin, S., Stanley, H. E. & Goldberger, A. L. *Chaos* **5,** 82–87 (1995).
6. Aghili, A. A., Rizwan-uddin, M., Griggin, P. & Moorman, J. R. *Phys. Rev. Lett.* **74,** 1254–1257 (1995).
7. Kitney, R. I., Linkens, D., Selman, A. C. & McDonald, A. H. *Automedica* **4,** 141–153 (1982).
8. Panter, D. *Modulation, Noise and Spectral Analysis* (McGraw-Hill, New York, 1965).
9. Akselrod, S. *et al. Science* **213,** 220–222 (1981).
10. Grossmann, A. & Morlet, J. *Mathematics and Physics, Lectures on Recent Results* (World Scientific, Singapore, 1985).

11. Daubechies, I. *Comments Pure Appl. Math.* **41,** 909–996 (1988).
12. Muzy, J. F., Bacry, E. & Arneodo, A. *Int. J. Bifurc. Chaos* **4,** 245–302 (1994).
13. Arneodo, A., Bacry, E., Graves, P. V. & Muzy, J. F. *Phys. Rev. Lett.* **74,** 3293–3296 (1995).
14. Vainshtein, L. A. & Vakman, D. E. *Separation of Frequencies in the Theory of Oscillations and Waves* (Nauka, Moscow, 1983).
15. Gabor, D. *J. Inst. Elect. Eng.* **93,** 429–457 (1946).
16. *MIT-BIH Polysomnographic Database* CD-ROM 2nd edn (MIT-BIH Database Distribution, Cambridge, 1992).
17. Guilleminault, C., Connolly, S., Winkle, R., Melvin, K. & Tilkian, A. *Lancet* **(I),** 126–131 (1984).
18. Stauffer, D. & Stanley, H. E. *From Newton to Mandelbrot: A Primer in Theoretical Physics* 2nd edn (Springer, Heidelberg, 1996).
19. Barabási, A.-L. & Stanley, H. E. *Fractal Concepts in Surface Growth* (Cambridge Univ. Press, 1995).
20. Kertész, J. & Vicsek, T. *Fractals in Science* (eds Bunde, A. & Havlin, S., (Springer, Heidelberg, 1994).
21. Stratonovich, R. L. *Topics in the Theory of Random Noise* Vol. I (Gordon & Breach, New York, 1981).
22. Lipsitz, L. A. *et al. Br. Heart J.* **74,** 340–396 (1995).
23. Gerstein, G. L. & Mandelbrot, B. B. *Biophys. J.* **4,** 41–68 (1964).

ACKNOWLEDGEMENTS. We thank L. A. N. Amaral for discussions. This work was supported by NIH, NIMH, NASA and The G. Harold and Leila Y. Mathers Charitable Foundation.

CORRESPONDENCE should be addressed to P.Ch.I. (e-mail: plamen@buphy.bu.edu).

A mechanism for halogen release from sea-salt aerosol in the remote marine boundary layer

Rainer Vogt*†, Paul J. Crutzen* & Rolf Sander‡

* Max-Planck-Institute for Chemistry, Air Chemistry Division, PO Box 3060, D-55020 Mainz, Germany
‡ Department of Chemistry and Centre for Atmospheric Chemistry, York University, North York, Ontario M3J 1P3, Canada

Recent measurements of inorganic chlorine gases[1] and hydrocarbons[2] indicate the presence of reactive chlorine in the remote marine boundary layer; reactions involving chlorine and bromine can affect the concentrations of ozone, hydrocarbons and cloud condensation nuclei. The known formation mechanisms of reactive halogens require significant concentrations of nitrogen oxides[3–5], which are not present in the unpolluted air of the remote marine boundary layer[6]. Here we propose an autocatalytic mechanism for halogen release from sea-salt aerosol: gaseous HOBr is scavenged by the aerosol and converted to only slightly soluble BrCl and Br_2, which are released into the gas phase. Depending on the sea-salt concentration and given a boundary layer that is stable for a few days, gaseous HOCl and HOBr may reach molar mixing ratios of up to 35 pmol mol^{-1}. We calculate that HOBr and HOCl are responsible for 20% and 40%, respectively, of the sulphur (IV) oxidation[7,8] that occurs in the aerosol phase. The additional S(IV) oxidation reduces the formation of cloud-condensation nuclei, and hence the feedback between greenhouse warming, oceanic DMS emission and cloud albedo. We also calculate significant bromine-catalysed ozone loss.

Recently, considerable attention[9–13] has been given to the role in the chemistry of the marine boundary layer (MBL) of chlorine atoms, which react with alkanes up to two orders of magnitude faster than do hydroxyl radicals. Chlorine atoms may accordingly serve as an additional oxidant, at concentrations larger than 1×10^3 atoms cm^{-3}. From diurnal measurements of non-methane hydrocarbons[2,14], or the observation of inorganic chlorine gases, Cl-atom concentrations of the order of 10^4–10^5 atoms cm^{-3} were inferred. In addition, Barrie *et al.*[15] have suggested—and there is now evidence for this from field measurements[16]—that ozone is destroyed in the MBL during polar sunrise by a mechanism involving Br and BrO.

So far no satisfactory mechanism has been proposed for reactive bromine and chlorine production in the pristine MBL or the Arctic. The gas-phase reactions of OH radicals with HCl or HBr are only a minor source of halogen atoms. Singh and Kasting[17] calculated Cl-atom concentrations of 10^3 atoms cm^{-3}, assuming an HCl volume mixing ratio of 1 nmol mol^{-1}, which is much larger than measured in the remote MBL[1,2,18]. Very recently, Mozurkewich[19] suggested the reaction of peroxomonosulphuric (Caro's) acid (HSO_5^-) with sea-salt bromide as a source of elemental bromine in the Arctic. However, the mechanism is favoured by low temperatures and high SO_2 concentrations and by itself should not oxidize significant amounts of halides. Mozurkewich also discussed direct bromide oxidation through free radicals, such as OH or HO_2 in the sea-salt aerosol. However, none of these mechanisms is capable of significant chlorine atom production in the unpolluted MBL.

Our proposed mechanism for autocatalytic bromine and chlorine chemistry in the liquid and gas phase is shown in Fig. 1. Hypobromous acid, HOBr, which is formed through an initial bromide oxidation (see below), is scavenged by sea-salt aerosol. Because in sea water (and therefore also in the nascent sea-salt aerosol) the bromide to chloride ratio is ~1/700, HOBr reacts with Cl^-:

$$HOBr + Cl^- + H^+ \leftrightarrow BrCl + H_2O \qquad (1, -1)$$

Recently, Wang *et al.*[20] determined a lower limit of the BrCl hydrolysis rate constant, $k_{-1} \geqslant 1 \times 10^5\ s^{-1}$. From the equilibrium constant $K_{1eq} = 5.6 \times 10^4\ M^{-2}$ (ref. 20), we calculate the rate constant of the forward reaction $k_1 \geqslant 5.6 \times 10^9\ M^{-2}\ s^{-1}$, which is of the same order of magnitude as that of the comparable reaction of HOBr with Br^- (ref. 21).

$$HOBr + Br^- + H^+ \leftrightarrow Br_2 + H_2O \qquad (2, -2)$$
$$(k_2 = 1.6 \times 10^{10}\ M^{-2}\ s^{-1},\ k_{-2} = 110\ s^{-1})$$

This reaction has been discussed as potentially important for bromine cycling on sulphate aerosol[22] and for autocatalytic bromine release from sea-salt aerosol[19,23]. Because of the large $[Cl^-]/[Br^-]$ ratio in sea water, the forward reaction (1) is much more important than forward reaction (2). Although the hydrolysis reaction (−1) is faster than reaction (−2), this is of lesser significance because a substantial fraction of the BrCl will react with Br^- leading to autocatalytic Br activation:

$$HOBr + Cl^- + H^+ \leftrightarrow BrCl + H_2O \qquad (1, -1)$$

$$BrCl + Br^- \leftrightarrow Br_2Cl^- \qquad (3, -3)$$

$$Br_2Cl^- \leftrightarrow Br_2 + Cl^- \qquad (4, -4)$$

$$Br_2 + h\nu \rightarrow 2Br \qquad (5)$$

$$2(Br + O_3) \rightarrow 2(BrO + O_2) \qquad (6)$$

$$2(BrO + HO_2) \rightarrow 2(HOBr + O_2) \qquad (7)$$

$$(\text{net})\,2HO_2 + H^+ + 2O_3 + Br^- + h\nu \xrightarrow{HOBr,Cl^-} HOBr + 4O_2 + H_2O \qquad (8)$$

Equilibria (3) and (4) were found to be established very rapidly[20], probably at a diffusion-controlled rate. After escape of Br_2 to the gas phase, photolysis (5) and reactions (6), (7) and (1) an autocatalytic cycle of bromine activation is closed. Thus, bromide oxidation is driven by HO_2, O_3 and aerosol acidity in the presence of sunlight and is catalysed by HOBr and Cl^-.

We have incorporated reactions (1)–(7) into a photochemical box model of the MBL[23]. The model treats chemical reactions in the gas phase and deliquesced sea-salt particles, as well as exchange between the two phases; standard O_3–NO_x–HO_x–S

† Present address: Ford Forschungszentrum Aachen, Dennewartstrasse 25, D-52068 Aachen, Germany.